Electronic Supplementary Material (ESI) for Environmental Science: Atmospheres.

Supporting Information

Oxidative Potential of Fine Particulate Matter Emitted from Traditional and Improved Biomass Cookstoves

Bradley H. Isenor[†§], Jillian P. Downey[†§], Samuel A. Whidden[†], Megan M. Fitzgerald[†‖], and Jenny P.S. Wong[†*]

[†]Department of Chemistry & Biochemistry, Mount Allison University, Sackville, Canada

[§]Now at: Department of Chemistry, University of Toronto, Toronto, Canada

[‖]Now at: Department of Chemistry, Memorial University of Newfoundland, St. John's, Canada

*Corresponding author: Jenny P.S. Wong (jwong@mta.ca)

Number of Pages: 13

Number of Figures: 5

Number of Tables: 4

Section 1. Cookstoves

The cookstoves were chosen to represent a range in cookstove technology (*i.e.*, traditional, natural- and forced-draft), and based on availability.

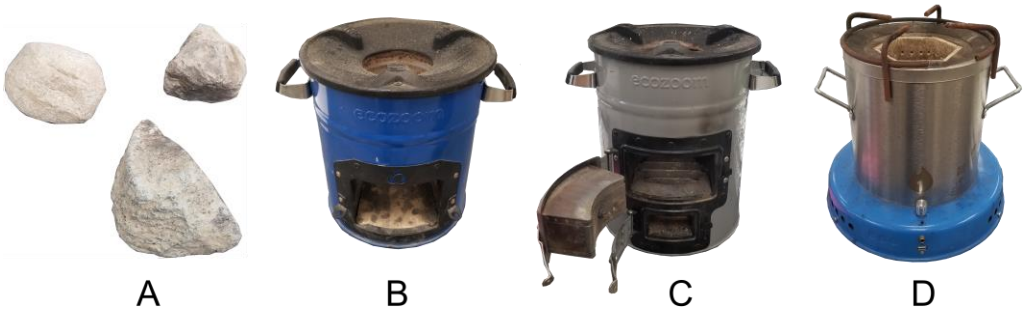

Figure S1. Pictures of cookstoves tested: **(a)** three-stone fire (TSF) traditional cookstove, **(b)** EcoZoom Dura, **(c)** EcoZoom Versa, and **(d)** African Clean Energy (ACE) One.

A. Three-Stone Fire Traditional Cookstove

The three stone fire is the most common traditional cooking method and in this study, the "minimally tended" three-stone fire was used where fuel was loaded in batches approximately every 10 minutes, which is considered to be more representative of real-world cooking practices compared to the "carefully tended" three-stone fire.[1]

B. EcoZoom Dura

A natural-draft rocket improved cookstove with a fully insulated stove body using ceramic that is lined with a refractory metal and a three-pronged cast iron top. The stove, as per the manufacturer's catalogue, can be used with wood and other solid biomass fuels and has a thermal efficiency of 27%, an ISO-IWA cookstove performance tier 2 for high power thermal efficiency and tier 1 for safety.[2] Retail cost is approximately US $35.

C. EcoZoom Versa

A natural-draft rocket improved cookstove with a fully insulated stove body using lightweight ceramic fibers that is lined with a refractory metal and a three-pronged cast iron top. A bottom damper door regulates air flow and a main combustion door. Both doors were opened for all testing. According to the manufacturer website, the stove can be used with wood and other solid biomass fuels and has a thermal efficiency of 38%.[2] Retail cost is approximately US $80.

D. African Clean Energy (ACE) One

A forced-draft gasifier stove with a fan that is powered by a rechargeable battery. The fan provides a forced-draft air that is introduced into the top and bottom of the combustion chamber through various holes. The fan setting is user-defined, and the middle setting was used. The stove is ceramic-lined and can burn any solid biomass fuel. As reported by the Clean Cooking Catalog, the thermal efficiency of the ACE One is 41.5%.[3] Retail cost is approximately US $150.

Note that we attempted testing of an artisan traditional clay stove, but the corresponding burn events resulted in cooking pot water temperatures more than 6 degrees below its boiling point, so the resulting data were excluded from all analysis as the lowered temperature rendered the test invalid according to the temperature criteria of the water boiling test.

Section 2. Fuels

Unless specified, all fuels were used as received. The moisture content was determined from ten different fuel pieces and measured using Toptes Pin-type moisture meter TS-630.

Split Dry Hardwood

"Xtraflame" kiln-dried hardwood from Charbonneau Floral Ltd (Laval, Quebec) was used and was cut using a table saw into approximately 3.5 cm × 3.5 cm × 5.0 cm pieces. The average moisture content is 10.8%. It has been reported that Charbonneau Floral mainly harvest hardwood types such as maple, birch, and beech, which were likely the hardwoods used in this study.[4]

Charcoal Briquettes

Compressed hardwood charcoal briquettes by Royal Oak (Roswell, Georgia) were used. The dimensions of the charcoal briquettes were approximately 5 cm × 5 cm × 2.5 cm. The average moisture content is < 6.8 % (below the detection limit of the moisture meter).

Charcoal Lumps

Charcoal hardwood lumps by Maple Leaf (Sainte Christine, Quebec) were used. The dimensions of the charcoal lumps were non-unform in size, and pieces were selected to fit in the combustion chamber of each stove, with typical dimensions of 7 cm × 3 cm × 3 cm. The average moisture content is < 6.8 % (below the detection limit of the moisture meter).

Table S1. Mean (± 1 standard deviation) fuel consumption and ash residue for each cookstove-fuel combination tested.

Stove-Fuel Combination	Fuel Consumption (g/min)	Ash Residue (wt % of fuel used)
	Wood	
Three-Stone Fire	7.4 ± 0.7	11.7 ± 1.8
EcoZoom Dura	13.5 ± 0.5	2.6 ± 0.5
EcoZoom Versa	16.2 ± 1.3	2.8 ± 1.1
ACE One	9.7 ± 0.9	1.5 ± 0.3
	Charcoal Briquettes	
Three-Stone Fire	7.5 ± 0.3	52.6 ± 7.4
EcoZoom Dura	12.5 ± 3.1	46.8 ± 3.1
EcoZoom Versa	13.3 ± 1.1	42.4 ± 4.8
ACE One	9.5 ± 0.6	35.4 ± 6.5
	Charcoal Lumps	
Three-Stone Fire	4.4 ± 0.7	23.3 ± 6.0
EcoZoom Dura	6.7 ± 1.5	16.7 ± 1.5
EcoZoom Versa	8.2 ± 0.6	8.8 ± 7.4
ACE One	6.7 ± 0.6	16.7 ± 1.5

Section 3. Water-Soluble Inorganic Ion Measurements

1.5 cm^2 filter punch was extracted in a sterile tube containing 10 mL of purified water (Milli-Q; 18.2 $M\Omega\ cm^{-1}$) via sonication for 60 minutes. The resulting extract was filtered using a 0.45 µm pore size polytetrafluoroethylene (PTFE) syringe filter (VWR) to remove insoluble material. The filter extract was injected into an ion chromatography (IC) system (940 Professional IC Vario, Metrohm) coupled to an autosampler (858 Professional Sample Processor, Metrohm) to measure anions (F^-, Cl^-, NO_2^-, Br^-, NO_3^-, SO_4^{2-}, and PO_4^{3-}) and cations (Li^+, Na^+, K^+, Ca^{2+}, Mg^{2+}, and NH_4^+) using A Supp 5 column (150 × 4.0 mm, Metrohm) and C4 column (150 × 4.0 mm, Metrohm), respectively. The anion eluent (flow rate: 0.9 mL/min) is 1.7 mM HNO_3 (ultra-trace grade, VWR) and 0.7 mM dipicolinic acid (> 99%, Sigma Aldrich) and the cation eluent (flow rate: 0.7 mL/min) is 3.2 mM sodium carbonate and 1.0 mM sodium bicarbonate (A Supp 5 Eluent concentrated snips, Metrohm); both eluents were prepared using purified water. The sample loop volume of 20 µL and the IC system was calibrated using varying standards (0.005 – 50 ppm) that were prepared using NIST-traceable reference material.

Section 4. QA/QC of OC, EC, and Inorganic Ion Data

OC/EC Measurements

The method detection limit (MDL) for the OC and EC measurements was 2.2 $\mu g/m^3$, calculated as three times the standard deviation of replicate blank measurements (reported by the Sunset Laboratories Inc.) and using the mean air volume sampled for cookstove filters of 0.6 m^3. 11 filters (7 front filters and 4 back filters) were measured in duplicate and coefficient of variation for these replicate measurements are 0.3–5.7% for OC and 0.2–24% for EC (the high coefficient of variation for EC is due to low EC mass loading on two back filters that were slightly above the MDL).

Inorganic Ion Measurements

Quintuplet measurements of blank quartz filters were carried out to determine the MDL, which was calculated as three times the standard deviation of these blank measurements. Using the mean air volume sampled for cookstove filters of 0.6 m^3, the MDL ($\mu g/m^3$) was determined as follows: F^- (1.90), Cl^- (7.92), NO_2^- (13.13), Br^- (1.82), NO_3^- (5.69), SO_4^{2-} (15.36), PO_4^{3-} (3.15), Li^+ (0.27), Na^+ (9.12), K^+ (4.73), Ca^{2+} (14.02), Mg^{2+} (2.75), and NH_4^+ (1.30).

For all sample and back filter measurements below the MDL where the ion peak was detected, the measured value was replaced with MDL/$\sqrt{2}$. The ion concentrations of the back filter were accounted for, and if the back-filter corrected values were less than or equal to zero, they were replaced with zeros. Four sample filters were measured in triplicate and coefficient of variations of these replicate measurements are 3 – 13%.

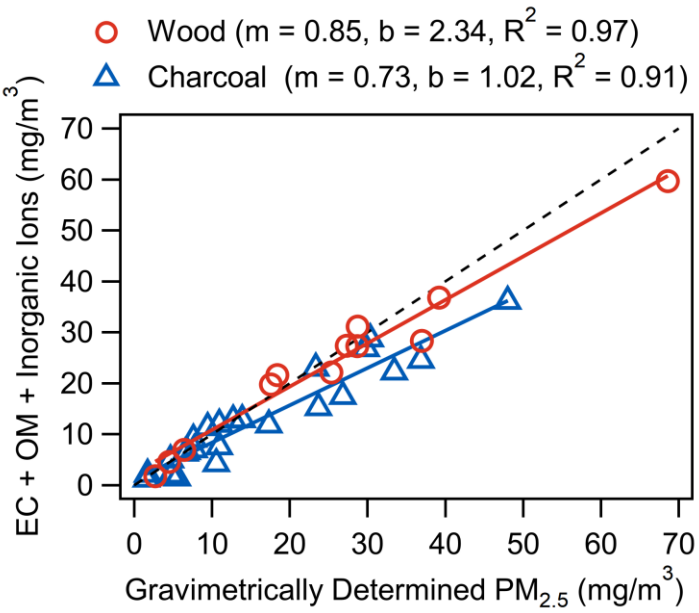

Figure S2. Gravimetrically determined $PM_{2.5}$ mass concentration versus the sum of EC, OM, and measured inorganic ion mass concentration for wood (red circles) and charcoal (blue triangles) fuels used in all cookstoves. The red and blue solid lines represent the line-of-best-fit for each fuel type, and the black dash line represents the 1:1 line.

Section 5. DTT Activity

Extraction: $PM_{2.5}$ filter punch (0.126–1.5 cm^2) were extracted in a sterile tube containing 15–50 mL of purified water (Milli-Q; 18.2 MΩ cm^{-1}) via sonication for 60 minutes. The filter punch area and purified water volume for extraction varied to yield an appropriate DTT decay rate (*i.e.*, sufficient measurements to fit a linear regression of DTT concentration over reaction time). The DTT decay rate is also commonly referred to as DTT activity. For water-soluble (WS) DTT activity, a portion of the extract was removed and filtered using a 0.45 μm pore size polytetrafluoroethylene (PTFE) syringe filter (VWR) and 2.45 mL of this filtered solution was used for the DTT assay. For total-DTT activity, 2.45 mL of the unfiltered sample extract with the filter punch remaining in the solution was used.

Incubation: The following was added to both WS- and total PM extract and the resulting mixtures were incubated at 37 °C in a dry heat bath: 0.7 mL of 0.5 M potassium phosphate buffer (pH 7.4; VWR; trace metals removed using a Chelax-100 [Sigma Aldrich] column) and 0.35 mL of 1 mM DTT (98%, Sigma Aldrich) to initiate the reaction of DTT with $PM_{2.5}$ components.

Reaction Quenching and Monitoring: At different reaction times over 46 minutes, 100 μL of the incubation mixture was removed and added to separate vial containing 1 mL trichloroacetic acid (1% w/v TCA) to quench the reaction between DTT and $PM_{2.5}$ components. The concentration of DTT was determined by adding 2 mL of 0.08 M Tris buffer (VWR) containing 4 mM ethylenediaminetetraacetic acid (EDTA; >99.4%, Sigma Aldrich) at pH 8.9 and 0.5 mL of 0.2 mM 5,5'-dithiobus(2-nitrobenzoic acid) (DTNB; 99%, Alfa Aesar). Under high pH conditions, the DTNB reacts with the unreacted DTT to form the light absorbing product 2-nitro-5-thiobenzoic acid, which can be detected at 412 nm. Two separate absorption spectrophotometers were used, the Cary 100 UV-Vis (Agilent) and another absorption spectrophotometer that consists of liquid wavelength capillary cell (10 cm, World Prevision Instrument), a deuterium tungsten light source (DT-Mini-2, Ocean Optics), and a multi-wavelength detector (USB2000+, Ocean Optics). Absorbance at 412 nm was corrected for small fluctuations in baseline by subtracting the absorbance at 700 nm, given that 2-nitro-5-thio benzoic acid does not absorb at this higher wavelength.[5] Each UV-VIS spectrometer was calibrated routinely using freshly prepared solutions of DTT.

Controls and Corrections: Since DTT itself is an unstable compound, its decay in purified water (with no PM) was determined and accounted for. In order to evaluate the day-to-day reproducibility of the DTT assay, two positive controls using 9,10-phenanthrenequinone (PQN; 99%, Sigma Aldrich; final concentration 0.21 μM in the incubation vial) were also conducted for each assay. The coefficient of variation for all PQN positive controls is 19%.

The WS- and total-DTT activity for the back filter was also determined and accounted for by using the same punch size, extraction, and DTT assay protocol as those employed for the corresponding front filter (this correction on average is 17% of the uncorrected DTT activity).

Section 6. PLSR Models

Four and two components were selected for $OP_{vol}^{Total\text{-}DTT}$ and $OP_{vol}^{WS\text{-}DTT}$ PLSR models as this led to the lowest root mean squared error of prediction (RMSEP). While the RMSEP was minimized for six components for the $OP_{vol}^{WI\text{-}DTT}$ PLSR model, the four component model was chosen as 1) the increase in two more component only resulted in a small increase in the percentage (3.1%) of variance explained for the response variable, 2) to avoid overfitting, and 3) to maintain model simplicity.

The robustness of the developed PLSR models was assessed using two criteria: 1) the Q^2 value (average goodness of fit for all test folds; a measure of model predictive ability) was not more than 10% lower than the R^2 value (average goodness of fit of the model for all training folds; a measure of model explanation ability).[6] This suggests that the models did not overfit the training folds and can be used to predict the testing folds. 2) In permutation testing, the R^2 of the actual PLSR model was consistently greater than the R^2 of each PLSR model developed using randomly permutated OP_{vol}^{DTT} (1000 permutations). In particular, while the actual $OP_{vol}^{Total\text{-}DTT}$ and $OP_{vol}^{WI\text{-}DTT}$ PLSR models outperformed all 1000 permutated models (*i.e.*, passed all 1000 permutations), the actual $OP_{vol}^{WS\text{-}DTT}$ PLSR model was outperformed by only 8 out of 1000 permutated models. This suggests that the relationship captured by the PLSR $OP_{vol}^{WS\text{-}DTT}$ model is still highly robust and has significant predictive power.

Table S2. Performance assessment of PLSR models developed for $OP_{vol}^{Total\text{-}DTT}$, $OP_{vol}^{WS\text{-}DTT}$, and $OP_{vol}^{WI\text{-}DTT}$ using indicators R^2 (average goodness of fit of the model for all training folds); Q^2 (average goodness of fit for all test folds), and whether the developed model passed the permutation test (1000 permutations).

Model	R^2	Q^2	Permutation Results
$OP_{vol}^{Total\text{-}DTT}$	0.89	0.98	1000/1000
$OP_{vol}^{WS\text{-}DTT}$	0.68	0.98	992/1000*
$OP_{vol}^{WI\text{-}DTT}$	0.87	0.98	1000/1000

Note: *8 out of 1000 permutations failed.

We note that PLSR models including the unknown component were also developed to evaluate the role of unmeasured species on OP_{vol}^{DTT}. These PLSR models had similar predictive power and performance metrics compared to the PLSR models excluding the unknown component. The main findings, including VIP score rankings and coefficient magnitudes for predictors, remained largely unchanged as well. The notable exception is for the $OP_{vol}^{WI\text{-}DTT}$ model without the unknown component, where NO_2^- has lost its significance as a predictor. However, it is important to note that the magnitude of the coefficients for these inorganic ions remained small for both models with and without the unknown component (ranging from +0.03 to -0.02), which consistently suggest that they play a limited role in determining the DTT activity of water-insoluble component of cookstove $PM_{2.5}$.

Given the similar response for the PLSR models with and without the unknown component, the PLSR models without the unknown component were selected. In addition, the use of PLSR without the unknown component is also in line with previous literature where multivariate/regression models of DTT activity have utilized directly measured chemical species.[6–10]

Section 7. Measurements by Stove/Fuel Combination

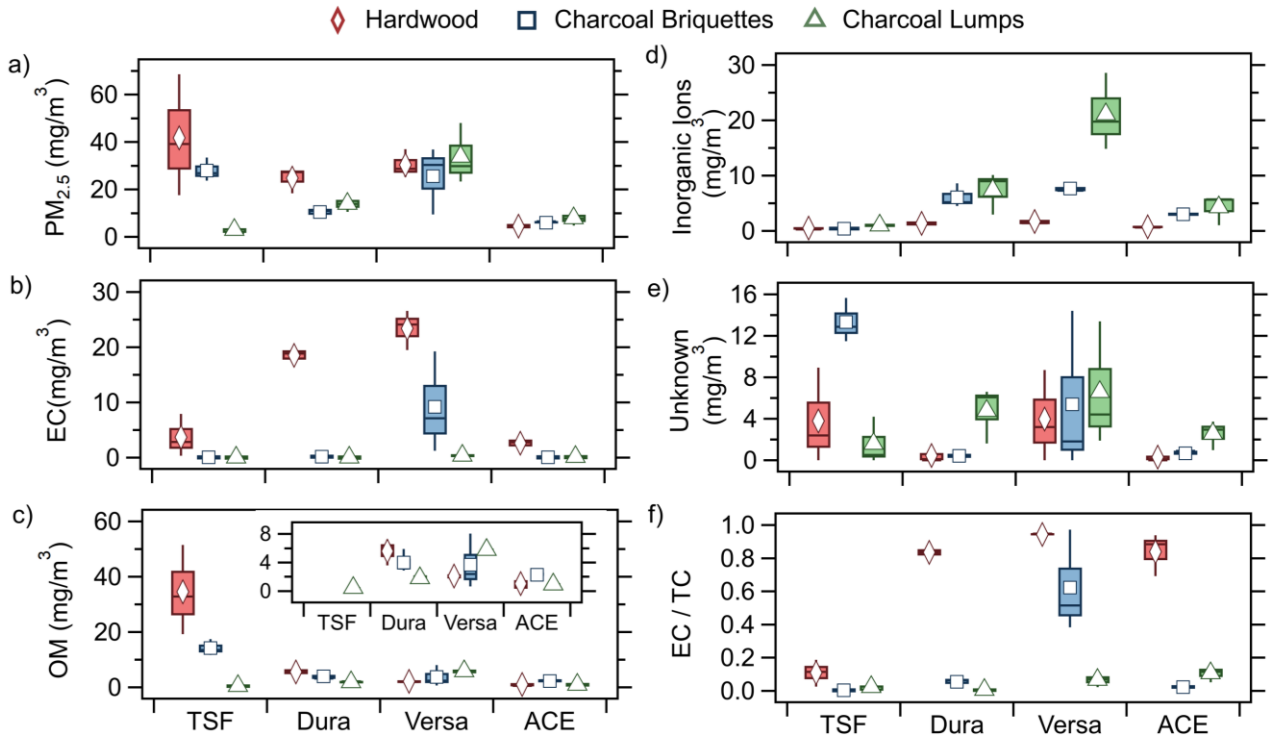

Figure S3. Box and whisker plots of the mass concentrations of **(a)** $PM_{2.5}$, **(b)** EC, **(c)** OM, **(d)** inorganic ions, and **(e)** unknown component, as well as **(f)** elemental carbon-to-total carbon (EC/TC) ratio for each stove/fuel combination. The horizontal line within the box indicates median values; the upper and low box boundaries represent the 75th and 25th percentile; the whiskers indicate 95th and 5th percentile; the red diamond, blue square, and green triangle markers indicates the mean for hardwood, charcoal briquettes, and charcoal lumps, respectively.

The increased EC contribution for Versa burning charcoal fuels (Figure 1b of the main text) was driven by high and variable EC mass concentration (1.2–19.2 mg/m^3; Figure S3b) when burning charcoal briquettes. We speculate that the variable EC mass for Versa burning charcoal briquette was due to the higher ash content of charcoal briquettes compared to the other fuels used (see Table S1). During the simmering phase, ash built-up near the damping door was observed, which potentially reduced air flow into the combustion chamber and led to more variable and lower combustion efficiency. The greater variability in OM mass concentration, as shown in Figure S3c, also supports the likelihood of variable combustion conditions.

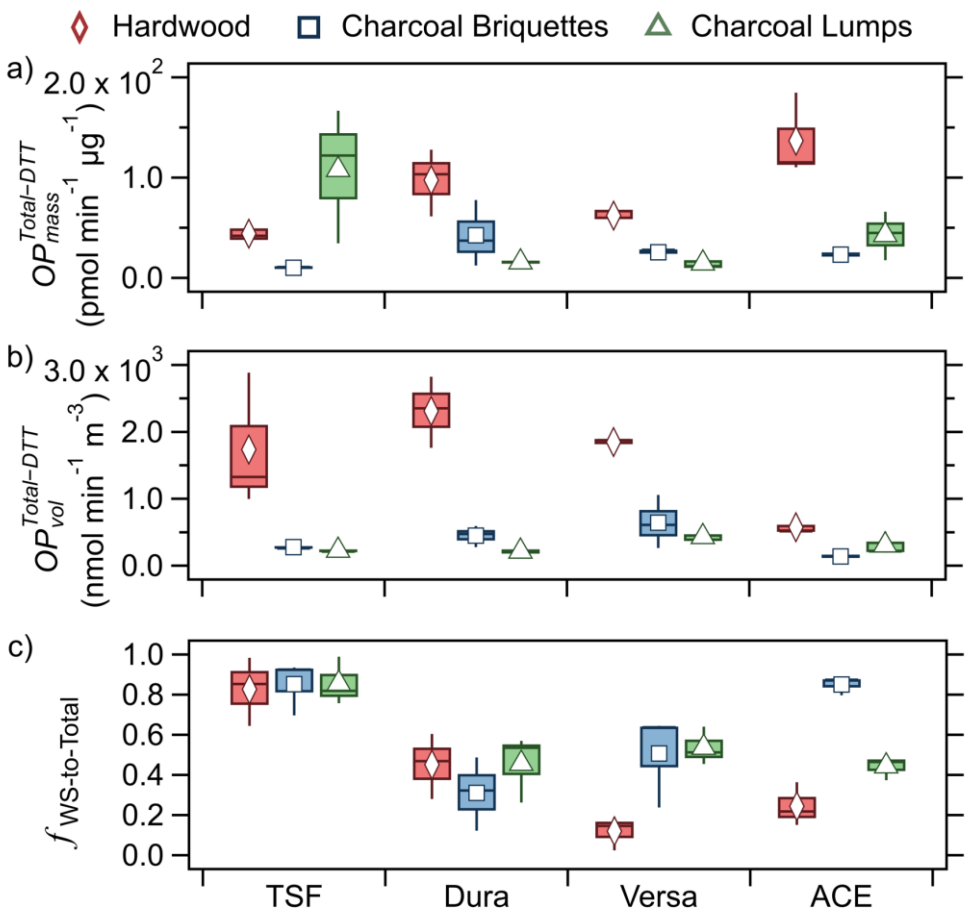

Figure S4. Box and whisker plots of **(a)** mass-normalized DTT activity ($OP_{mass}^{Total\text{-}DTT}$), **(b)** air volume-normalized total DTT activity ($OP_{vol}^{Total\text{-}DTT}$), and **(c)** ratio of water-soluble (WS) to total volume-normalized DTT activity ($f_{WS\text{-}to\text{-}Total}$) for each stove/fuel combination. The horizontal line within the box indicates median values; the upper and low box boundaries represent the 75th and 25th percentile; the whiskers indicate 95th and 5th percentile; the red diamond, blue square, and green triangle markers indicates the mean for hardwood, charcoal briquettes, and charcoal lumps, respectively.

Traditional stove burning wood resulted in significant contributions of WS fraction (0.83 ± 0.17) to $OP_{vol}^{Total\text{-}DTT}$, which is consistent with field samples of fresh biomass burning organic aerosol where $f_{WS\text{-}to\text{-}Total}$ is 0.82.[11] Considering only wood fuels, compared to TSF, all improved cookstoves had significantly lower mean $f_{WS\text{-}to\text{-}Total}$ (0.12–0.45). Amongst improved cookstoves, Dura had a statistically higher $f_{ws\text{-}to\text{-}total}$ (0.45 ± 0.16) compared to Versa, while similar fractional contributions were observed for Versa and ACE. For wood combustion, the trends in $f_{WS\text{-}to\text{-}Total}$ appear to align with the relative contribution of EC and OM to total $PM_{2.5}$ (Figure 1b of the main text). For TSF, $PM_{2.5}$ with proportionally more OM than EC corresponds to a higher $f_{WS\text{-}to\text{-}Total}$ whereas $PM_{2.5}$ from improved cookstoves is predominately EC, the corresponding $f_{WS\text{-}to\text{-}Total}$ is comparatively lower.

For charcoal fuels, only the natural draft stoves had statistically lower mean $f_{ws\text{-}to\text{-}Total}$ compared to TSF. When comparing the same cookstove type, only Versa and ACE had significant differences in mean $f_{ws\text{-}to\text{-}Total}$ between wood and charcoal fuels, where $f_{ws\text{-}to\text{-}Total}$ was greater when charcoal was burned.

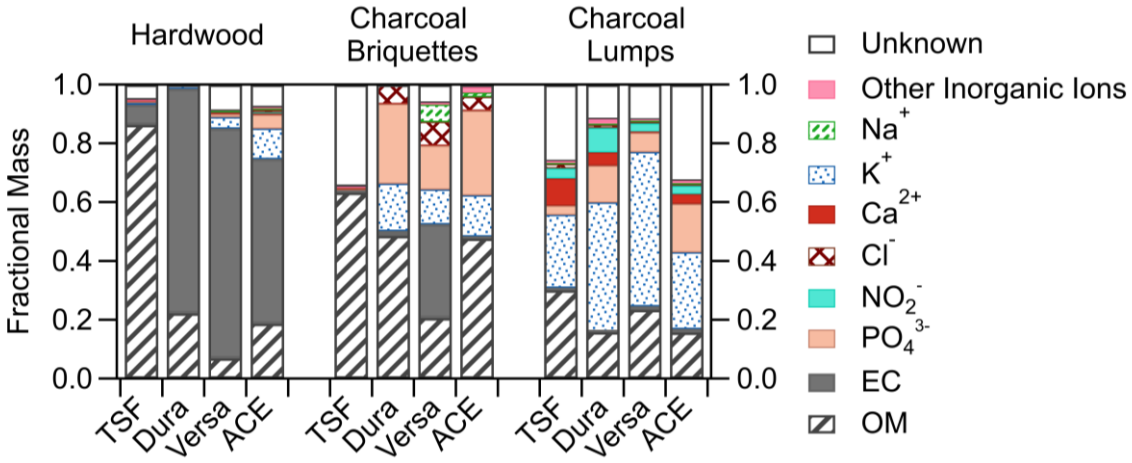

Figure S5. Mean fractional mass contribution of OM (stripped bar), EC (dark grey bar), inorganic ions (varying colour bars) and unknown (colourless bar) to $PM_{2.5}$.

Table S3. Spearman rank correlation coefficients (r_s) and significance values (p, 2-tailed) for correlations between $OP_{mass}^{Total\text{-}DTT}$ and mass fraction of EC, OM, and inorganic ions (measured chemical components/species).

Chemical Component	r_s	p
EC	+0.62	<0.01*
Li^+	+0.19	0.27
Cl^-	+0.17	0.33
Ca^{2+}	+0.14	0.43
Mg^{2+}	+0.05	0.77
Na^+	-0.03	0.86
NH_4^+	-0.07	0.68
NO_2^-	-0.08	0.64
SO_4^{2-}	-0.09	0.59
Br^-	-0.15	0.40
K^+	-0.16	0.35
PO_4^{3-}	-0.19	0.26
OM	-0.20	0.27
F^-	-0.20	0.24
NO_3^-	-0.30	0.08

Note: * denotes $p \leq 0.05$.

Table S4. Variable importance in projection (VIP) scores and corresponding regression coefficients for all predictors in all PLSR models of OP_{vol}^{DTT}. The predictors are listed in order of decreasing VIP scores for each PLSR model.

$OP_{vol}^{Total\text{-}DTT}$			$OP_{vol}^{WS\text{-}DTT}$			$OP_{vol}^{WI\text{-}DTT}$		
Predictor	**VIP**	**Coefficient**	**Predictor**	**VIP**	**Coefficient**	**Predictor**	**VIP**	**Coefficient**
EC	2.25	+0.70	OM	2.51	+0.64	EC	2.69	+0.88
OM	1.33	+0.53	PO_4^{3-}	1.15	-0.17	PO_4^{3-}	1.01	+0.03
PO_4^{3-}	1.20	-0.06	NO_2^-	1.10	+0.02	Mg^{2+}	1.00	-0.06
NO_2^-	1.10	-0.07	NO_3^-	1.04	+0.03	NH_4^+	0.97	-0.11
Ca^{2+}	1.02	-0.12	EC	1.03	+0.26	NO_2^-	0.96	-0.10
NO_3^-	1.01	+0.14	Ca^{2+}	0.95	-0.04	Ca^{2+}	0.95	-0.15
Mg^{2+}	0.93	-0.07	K^+	0.92	+0.03	NO_3^-	0.84	+0.21
K^+	0.87	0.00	F^-	0.78	+0.07	K^+	0.71	-0.02
NH_4^+	0.84	-0.16	NH_4^+	0.70	-0.11	F^-	0.66	-0.04
Na^+	0.57	+0.07	Mg^{2+}	0.64	-0.06	Br^-	0.52	-0.24
Br^-	0.50	-0.18	Li^+	0.52	+0.11	Na^+	0.51	+0.06
SO_4^{2-}	0.48	+0.08	SO_4^{2-}	0.46	+0.09	SO_4^{2-}	0.50	+0.10
Cl^-	0.42	-0.02	Cl^-	0.37	0.00	OM	0.47	+0.14
F^-	0.38	-0.08	Na^+	0.35	-0.03	Li^+	0.44	+0.02
Li^+	0.17	+0.06	Br^-	0.16	-0.02	Cl^-	0.37	-0.11

References

1) J. Jetter, Y. Zhao, K. R. Smith, B. Khan, T. Yelverton, P. DeCarlo and M. D. Hays, Pollutant Emissions and Energy Efficiency under Controlled Conditions for Household Biomass Cookstoves and Implications for Metrics Useful in Setting International Test Standards, *Environ. Sci. Technol.*, 2012, **46**, 10827–10834.

2) Ecozoom, Ecozoom Catalogue, https://ecozoomglobal.com/s/ecozoomstoves10_19-1.pdf, (accessed 7 July 2023).

3) Cleaning Cooking Alliance, Clean Cooking Catalog - ACE One, http://catalog.cleancookstoves.org/stove_details.html?stove_id=stove_0CBX51V, (accessed 7 July 2023).

4) J. Gagne, M. Al Zayat and D. Nisbet, *Firewood Pathway Analysis for Canada*, Invasive Species Centre, 2017.

5) T. Fang, V. Verma, H. Guo, L. E. King, E. S. Edgerton and R. J. Weber, A semi-automated system for quantifying the oxidative potential of ambient particles in aqueous extracts using the dithiothreitol (DTT) assay: results from the Southeastern Center for Air Pollution and Epidemiology (SCAPE), *Atmos. Meas. Tech.*, 2015, **8**, 471–482.

6) S. J. Campbell, K. Wolfer, B. Utinger, J. Westwood, Z.-H. Zhang, N. Bukowiecki, S. S. Steimer, T. V. Vu, J. Xu, N. Straw, S. Thomson, A. Elzein, Y. Sun, D. Liu, L. Li, P. Fu, A. C. Lewis, R. M. Harrison, W. J. Bloss, M. Loh, M. R. Miller, Z. Shi and M. Kalberer, Atmospheric conditions and composition that influence $PM_{2.5}$ oxidative potential in Beijing, China, *Atmos. Chem. Phys.* 2021, **21**, 5549–5573.

7) D. Paraskevopoulou, A. Bougiatioti, I. Stavroulas, T. Fang, M. Lianou, E. Liakakou, E. Gerasopoulos, R. Weber, A. Nenes and N. Mihalopoulos, Yearlong variability of oxidative potential of particulate matter in an urban Mediterranean environment, *Atmos. Environ.*, 2019, **206**, 183–196.

8) M. R. Perrone, I. Bertoli, S. Romano, M. Russo, G. Rispoli and M. C. Pietrogrande, $PM_{2.5}$ and PM10 oxidative potential at a Central Mediterranean Site: Contrasts between dithiothreitol- and ascorbic acid-measured values in relation with particle size and chemical composition, *Atmos. Environ.*, 2019, **210**, 143–155.

9) D. Gao, K. J. Godri Pollitt, J. A. Mulholland, A. G. Russell and R. J. Weber, Characterization and comparison of $PM_{2.5}$ oxidative potential assessed by two acellular assays, *Atmos. Chem. Phys.*, 2020, **20**, 5197–5210.

10) J. Shang, Y. Zhang, J. J. Schauer, S. Chen, S. Yang, T. Han, D. Zhang, J. Zhang and J. An, Prediction of the oxidation potential of $PM_{2.5}$ exposures from pollutant composition and sources, *Environ. Pollut.*, 2022, **293**, 118492.

11) J. P. S. Wong, M. Tsagkaraki, I. Tsiodra, N. Mihalopoulos, K. Violaki, M. Kanakidou, J. Sciare, A. Nenes and R. J. Weber, Effects of Atmospheric Processing on the Oxidative Potential of Biomass Burning Organic Aerosols, *Environ. Sci. Technol.*, 2019, **53**, 6747–6756.